Atmospheric Array Loss Statistics for the Goldstone and Canberra DSN Sites Derived from Site Test Interferometer Data

David D. Morabito* and Larry R. D'Addario†

ABSTRACT. — NASA is interested in using the technique of arraying smaller-diameter antennas to increase effective aperture in order to replace aging monolithic 70-m structures of the Deep Space Network (DSN). Downlink arraying using the 34-m-diameter and 70-m-diameter antennas is routinely performed by the DSN for certain missions. Future scenarios will include extending the technique to uplink arraying where a downlink signal may not necessarily be available for phasing the signals at the individual stations of the array. Atmospheric decorrelation degrades the arrayed signal, and it becomes more severe in high-frequency bands such as the uplink allocations near 34 GHz and 40 GHz. This article provides sufficient information for a flight project to statistically account for this effect in the design of a telecommunications link involving arrayed antennas in the DSN. The annual and monthly cumulative distributions of expected phasing loss have been derived from the data acquired by site test interferometers at the Goldstone and Canberra complexes. These phasing loss statistics have then been mapped into two-element and three-element amplitude fade (dB loss) statistics referenced at the DSN uplink frequencies of 7.15 GHz and 34.5 GHz and at an elevation angle of 20 deg for both Goldstone and Canberra DSN sites. We also discuss validation tests that ensure the integrity of the data.

I. Introduction

NASA is interested in using the technique of arraying smaller-diameter antennas to replace aging monolithic 70-m structures of the Deep Space Network (DSN). Downlink arraying using the 34-m-diameter and 70-m-diameter antennas is routinely performed by the DSN for certain missions. It is desirable to extend the technique to uplink arraying (or downlink arraying where a strong signal may not be available for phasing the received signals from the individual stations). Atmospheric decorrelation will then degrade the arrayed signal, and the degradation gets worse with increasing frequency.

NASA is currently characterizing atmospheric effects at all the DSN stations using site test interferometers (STIs). Those at the Goldstone and Canberra DSN stations have been operating for several years. The Madrid STI began data collection in August 2013. The details of these instruments have been previously described [1].

Two independent STIs have been operating at the Venus and Apollo antenna sites in Goldstone, California, to assess the suitability of Goldstone as an uplink array site and to statistically characterize atmospheric-induced phase fluctuations for application to Goldstone array link scenarios. An intercomparison of the data from these two STIs has been previously described [2]. They are separated by 12.5 km but produce consistently similar results, suggesting that the scale for the evolution of the turbulence is shorter than the separation between instruments. For this article, we will utilize only the data from the Apollo STI for the Goldstone statistics since most of the antennas available for arraying at Goldstone are located there, and the intercomparison conclusion showed that the data from one STI can easily be adjusted to conditions at other locations within the complex.

The main parameters of the Goldstone and Canberra STIs are provided below:

Canberra STI (delivered 2011)
- Wideband — Equal-arm white-noise interferometer
- Initiated data acquisition in May 2011
- Has three elements operating as of January 2012
- Latitude 35.40 deg S, longitude 148.98 deg E, altitude 692.0 m
- Baseline distance — 250 m
- Signal source — Optus D3 geostationary satellite, 156 deg E longitude
    - Frequency 11.95 GHz
    - Elevation angle 48.25 deg

Goldstone Apollo STI (delivered 2010)
- Wideband — Equal-arm white-noise interferometer
- Initiated data acquisition in September 2010
- Has three elements operating as of November 2011
- Latitude 35.16 deg N, longitude 243.125 deg E, altitude 951.5 m
- East–west baseline distance — 190 m
- Signal source — Ciel-2 geostationary satellite, 129 deg W longitude
    - Frequency 12.45 GHz
    - Elevation angle 47.0 deg

An introductory study of array loss was reported previously [4]. This article provides sufficient information concerning atmospheric decorrelation to enable a flight project to statistically account for this effect in the design of a telecommunications link involving two or more arrayed antennas at the Goldstone or Canberra DSN site at nominal uplink frequencies. The annual and monthly cumulative distributions of the zenith delay RMS have been derived from the data acquired by the STIs. These delay RMS statistics have been mapped into two-element and three-element expected signal loss at the DSN uplink frequencies of 7.15 GHz or 34.5 GHz and at an elevation angle of 20 deg for selected array configurations

at both the Goldstone and Canberra DSN sites. In addition to accounting for the array loss, the telecom engineer must also account for individual antenna atmospheric attenuation and atmospheric noise temperature statistics [3] when constructing a link budget.

This article discusses the atmospheric effects on arraying, including the procedures used to map STI measurements into array loss (Section II). We also discuss validation tests that ensure the integrity of the data (Section III). The monthly and annual cumulative distributions of expected array loss for existing and likely array configurations are presented in the form of tables (Section IV), similar to the treatment for single-antenna atmospheric effects in [3].

II. Atmospheric Effects on Arraying

A. Single Ground Antenna

The principal weather-related effects on the performance of telecommunications links involving a single ground antenna are (1) the atmospheric attenuation, and (2) noise temperature increase resulting from oxygen, water vapor, clouds, and rain. The two effects are related and a higher atmospheric attenuation produces a higher noise temperature contribution. These effects are described and their magnitudes documented in the *DSN Telecommunications Link Design Handbook* antenna performance modules [3,5–7]. Design control tables (DCTs) used for telecommunications links typically carry separate entries for atmospheric attenuation of the received or transmitted signal and the atmospheric noise contribution (in the receiver) as a function of elevation angle and weather condition (cumulative distribution).

B. Arrayed Antennas

For arrayed antennas on the ground, atmospheric decorrelation must also be accounted for in the link budgets. Currently this is handled in the project-based link budget tool, Telecom Forecast Predictor (TFP), via a separate row entry in the form of array loss in dB, which currently uses a conservative value of 0.3 dB for X-band downlink arraying.[1] For a downlink array where a sufficiently strong signal is available, the signal-combining hardware can adaptively correct for phase differences among the signals, eliminating most of the loss. For an uplink array (or a downlink array without a strong reference signal), the phase differences are unknown but the magnitude of the loss can be inferred from tables such as those presented in this article. Methods to calculate array loss due to atmospheric decorrelation are presented here and closely follow the treatment discussed in previous articles [4,9].

C. Calculating Array Loss from STI RMS Delay Measurements

The processing of the STI data will be briefly discussed here. The design of the STIs deployed at the Goldstone Apollo, Canberra and Madrid sites is described in detail elsewhere [2,8].

---

[1] Chi-Wung Lau, personal communication, Communications Architectures and Research Section, Jet Propulsion Laboratory, Pasadena, California, 2013.

3

The raw STI data are recorded in the form of in-phase (I) and quadrature (Q) signal components at 0.1 s time resolution. The processing software first converts these signal components to phase and removes cycle ambiguities. The phase is filtered to remove long-term trends of satellite motion and instrumental drift. The remaining fluctuation energy is dominated by the troposphere over timescales ranging from about 1 s to several hundred seconds. The RMS scatter in these residual phases is then calculated for each 10-min interval. The STI RMS phase data are converted to RMS delay scatter and scaled from the elevation angle of the STI to obtain RMS delay at zenith. Thus, the final product of this first stage of data processing is 144 blocks zenith RMS delay measurements per day. Detailed discussion of the processing techniques and rational is provided in [2].

Atmospheric decorrelation statistics are provided in the form of cumulative distributions (CDs) of zenith delay RMS. A CD of 0.90 ("90 percent weather") means that 90 percent of the time a particular weather effect (noise temperature, attenuation, or atmospheric decorrelation) is less than or equal to the given value. Conversely, that value is exceeded 10 percent of the time.

Once the zenith RMS delay value for a particular site and CD is determined in the form of tabular data, this information can be used to estimate array loss for a particular array configuration after appropriate adjustments are made for elevation angle, link frequency, array element spacing, and site altitude. To convert this information to that of a particular array configuration of N antennas at a particular frequency and elevation angle, the following procedure is recommended [4,9]:

(1) Locate the monthly or yearly zenith delay RMS value σ_{τ_z} at the percentile of interest from the zenith delay RMS table applicable to the DSN site (see Section IV).

(2) Translate to the phase at the frequency of interest, f: $\sigma_{\phi_z} = 2\pi f \sigma_{\tau_z}$ (radians).

(3) Translate to the elevation angle θ of interest $\sigma_\phi = \sigma_{\phi_z} / \sin(\theta)^\gamma$ (radians). The exponent γ depends on the spacing between antennas relative to this height of the turbulent layer of the troposphere [10]. For Goldstone and Canberra, we adopt $\gamma = 1/2$, with the caveat that during the cold winter nights in Goldstone, γ is closer to unity. However, $\gamma = 1/2$ results in a conservative estimate and is applicable for most situations, so that value will be used throughout this article.

(4) Translate from STI baseline length r_{sti} to the separation between the elements of the array of interest as follows: $\sigma_{\phi_{ij}} = \sigma_\phi (r_{ij} / r_{sti})^{\beta/2}$, where r_{sti} equals 190 m for the east–west Goldstone Apollo baseline and 250 m for the Canberra east–west baseline and r_{ij} is the spacing between element numbers i and j of the array. Do this for all possible pairs $i \neq j$. See Table 1 for the element pair separation of specific DSN antennas. For the purpose of this study, we assume a thick-screen model of the turbulent layer ($\beta = 5/3$) [2].

(5) Note that there may be an additional adjustment if the height above mean sea level of the array is significantly different from that of the STI. For instance, the array involving DSS-14 and DSS-15 at Goldstone lies at an altitude of 1001 m and the STI at Goldstone Apollo lies at an altitude of about 951.5 m. To translate the Apollo STI phase RMS to the altitude of the DSS-14/DSS-15 array, we would use

$\sigma_{\phi_{ij}} e^{(h - ho)/H}$, where h = 951.5 m, ho = 1001 m, and H = 2 km [2]. This correction is not as important for Canberra where all of the antennas within the complex are located at similar heights.

(6) Finally, we calculate the expected value of the array loss as [9]:

$$\text{Expected Array Loss (dB)} = -10 \log \left[\frac{1}{N^2} \sum_{i=1}^{N} \sum_{j=1}^{N} \exp \left(-\left(\frac{\sigma_{\phi_{ij}}^2}{2} \right) \right) \right], \quad (1)$$

where $\sigma_{\phi_{ij}} = 0$ when $i = j$. The loss is with respect to the power received at a distant target from an array of identical elements whose signals are in phase at the target.

It must be emphasized that Equation (1) gives the expected value of the loss, and that its cumulative distribution describes the variation of that expected value as conditions change during a month or year. It does not give the probability distribution of the instantaneous loss, which is sometimes larger and sometimes smaller than the expected value. That probability distribution will be the subject of a follow-up article.

A list of DSN antenna pairs and their separations is provided in Table 1 for element spacing less than 1 km. The separations were calculated from coordinates provided in the *DSN Telecommunications Link Design Handbook*, Module 301 [11].

Table 1. Deep Space Station (DSS) station pair separations.

DSS	DSS	Separation, m
Goldstone		
24	25	258.4
24	26	494.0
25	26	302.0
14	15	497.8
Canberra		
34	35	302.5
34	36	488.5
34	45	389.1
35	36	276.0
35	45	452.1
36	45	380.7
34	43	442.3
35	43	735.8
36	43	849.9
43	45	547.5

III. Validation

This section describes various studies and demonstrations that have been conducted to validate the STI delay RMS presented here as being atmospheric in nature, consistent with estimates from other techniques, and thus usable for estimating array loss.

A. Evidence for STI Delay RMS Being Atmospheric in Nature

Several checks were made on the STI RMS delay data to verify that they were dominated by tropospheric effects. One such check involved examining the STI phase variations between seasons and between day and night. One component of this study involved selecting two days of data from the Goldstone STI data archive for detailed analysis: one cold weather day on December 11, 2008, where amplitude fluctuation effects due to troposphere were expected to be near minimum, and one warm (hot, humid) weather day on August 29, 2008, where such effects were expected to be near maximum [4]. These two cases were expected to provide the extreme conditions or range over which phase decorrelation can be characterized and were found to be consistent with expectations. The magnitude of the delay RMS fluctuations for the entire data set displayed expected seasonal and diurnal variations that also correlated well with measurements from surface meteorological data collected at the site. For instance, the Goldstone delay RMS measurements were highest during the hotter, more humid summer days and were lowest during the colder, less humid winter days. The day–night variation in delay RMS was strongest during summer (higher RMS delay near local noon), and weaker during winter [4].

In addition, the structure functions extracted from the STI data were examined to correlate their measured parameters with known atmospheric conditions. The slopes of the structure functions over short time scales (prior to the knee) all took values between the theoretical thick-layer model and thin-layer model limits expected for the atmosphere. It was further observed that the slopes reached their thick-layer model limit during the hottest Goldstone summer days and thin-model limit during the coldest Goldstone winter nights. The Goldstone structure function slopes exhibited a strong seasonal dependence characteristic of the desert climate. Most of the time, the structure function slope was found to take values in between these two limits. For Canberra, the structure function slopes lay just below the thick-layer model limit, exhibiting less variation with season than the corresponding Goldstone values. Other parameters extracted from the structure functions were also found to correlate with weather such as wind speed with time scale at the knee, and magnitude of the fluctuations with weather conditions (higher during hotter and more humid periods and lower during cooler and drier periods) [2,12].

B. Comparison of STI Delay RMS with That Measured with Other Instruments

In August 2008, dual water vapor radiometers (DWVRs) were deployed next to each antenna element of the STI residing at the Goldstone Venus site (location of the 34-m-diameter R&D antenna) forming a baseline of similar length [13]. The DWVRs were pointing in the direction of the STI satellite in the sky. The use of two WVRs allows estimation of their differenced path delay fluctuations, which produces a data type that could be compared directly against the STI phase difference fluctuations (after filtering out longer-period nontroposphere variations).The results of this intercomparison showed that differenced path delay fluctuations measured from the two WVRs were comparable with and correlated well with the delay RMS fluctuations from the STI [13].

C. Comparison with Array Loss Inferred from Uplink 7.15-GHz Array Demos

A series of uplink array demonstrations conducted at X-band [14–16] suggested that the inferred level of atmospheric loss was very low, no more than 0.2 dB. This limit is consistent with predicted array gain based on the range of expected values extracted from the STI data reported on in this article for the vast majority of CD values.

D. Comparison with Array Loss Derived from Downlink 32-GHz Array Demos

It was desired to statistically validate fades predicted from STI data by performing uplink arraying demos and comparing with measured fades. Since such fades at 7.15 GHz are usually much too small to measure (see Section III.C), it was decided to conduct such demonstrations at higher frequencies where the expected magnitudes of such fades are much larger and thus measurable. However, since the uplink arraying infrastructure is not currently available for the 34-GHz uplink band, we conducted demonstrations using downlink arraying at the nearby 32-GHz band using the operational processing equipment with adaptive phase adjustment turned off. We also recorded the individual received signals at each antenna and estimated the array loss from the phase differences extracted from the data.

A series of such demonstrations was performed using the Cassini spacecraft's 32-GHz carrier with antennas residing at the Apollo 34-m subnet at Goldstone, where the STI resides. Downlink array demo passes using Cassini were conducted in June 2012, July 2013, and August 2013 in order to measure signal fades that can be compared with estimates derived from STI data acquired during the same period. Fades were determined for the DSN antenna array either by using the array-processing hardware (with adaptive correction off) or by differencing phases measured by open-loop receivers connected to the individual antennas. The antennas involved in the array were DSS-25 and DSS-26. The STI continuously observes geostationary satellites that remain in the same location in the sky while the arrayed steerable DSN antennas track planetary spacecraft across the sky. The STI delay RMS values were converted to conditions of the spacecraft tracked by the DSN array by adjusting the frequency, elevation angle, and projected baseline length making use of the geometric profile of the spacecraft being tracked by the DSN stations. It was found that the statistics of the phase delay RMS signature from the STI were consistent with the statistics of the magnitude of the phase difference of the DSS-25/DSS-26 array. The fade signatures of the two instruments were not expected to exactly line up since the STI's geostationary satellite and the array's spacecraft did not lie in the same raypath as the signals were propagating through different atmospheric cells. However, when Cassini (as observed by the DSS-25/DSS-26 array) was located in the same general direction in the sky as the Ciel-2 geostationary satellite (observed by the STI), the STI and arrayed DSS-25/DSS-26 phase variations were statistically similar and their time series showed periods of high correlation, including delayed features as expected. The detailed results of this study will be reported on in a future article.

IV. CD Plots and Tabular Data

The model presented here is based on STI data acquired at Goldstone and Canberra during 2011, 2012, and 2013. (The Madrid STI has not yet collected enough data for statistical characterization and will be reported on in a future article.) This model contains 32 months

of Goldstone data from January 2011 through August 2013, and 28 months of Canberra data from May 2011 through August 2013. As more years of data are collected, they will be incorporated and updated tables will be published.

Both the Canberra and Goldstone STIs are three-element instruments. Data acquired to date on all three baselines at each site show that the delay RMS statistics from each baseline are very similar to those of the other two. Therefore, for this analysis we have chosen to use the statistics from only the east–west baseline at each site with the expectation that the statistics will not vary significantly with the inclusion of the data from the other two baselines for each site [2].

In addition, several additional years of data were acquired from the Venus Goldstone site [17–21], which has operated since May 2007. Analysis shows that the Venus data are consistent with the Apollo data after adjusting for the differences in STI separation and site altitude [2]. The Venus data are not included in this analysis.

A. Goldstone Apollo Complex

Delay RMS Statistics

The statistics of the zenith RMS delay were generated for each month of STI data and are presented in a format similar to the single antenna attenuation and atmospheric noise temperature tables in the *DSN Telecommunications Link Design Handbook* [3]. The monthly and yearly delay RMS statistics referenced to zenith are presented in Table 2 for the Goldstone Apollo DSN site as extracted from the east–west STI baseline data. The smallest delay RMS, 0.061 ps, occurred in November. It is comparable to the ~0.1 ps instrumental noise level. The summer months have minimum RMS values ~0.2 ps, suggestive of higher instrumental noise or atmospheric effects peaking above the ~0.1 ps instrumental noise level. August has the highest delay RMS at about 7.97 ps. The 90 percent year average zenith delay RMS is about 2.24 ps.

Figure 1 displays the monthly CD curves for the zenith delay RMS extracted from the east–west STI baseline data. Note the strong seasonal separation between the CD curves that is characteristic of the Goldstone desert climate. The summer month curves all lie at the right, with the winter month curves at the left. There is also a day/night variation (not shown) which is observed to be stronger in the summer months.

Figure 2 displays the CDs of zenith delay RMS for the warm summer months at Goldstone from individual years including the composite CD curve for that month (also shown in Figure 1). There is a reasonable degree of consistency between the individual year CDs and the composite CD for each month, with the spread being much less for September and a little larger for the other summer months. Note that August 2012 appears to be the most active month, showing the highest delay RMS for a given CD value. The 90 percent values of the composite CD curves for the summer months lie in between 2.7 and 3.3 ps.

Table 2. Zenith delay RMS in ps, Goldstone, 190-m baseline.

CD	Jan	Feb	Mar	Apr	May	Jun	Jul	Aug	Sep	Oct	Nov	Dec	Year Min	Year Avg	Year Max
0.00	0.080	0.097	0.083	0.081	0.092	0.094	0.174	0.210	0.162	0.074	0.061	0.088	0.061	0.108	0.210
0.10	0.224	0.265	0.297	0.361	0.424	0.471	0.660	0.628	0.519	0.265	0.240	0.225	0.224	0.382	0.660
0.20	0.288	0.344	0.423	0.490	0.559	0.625	0.835	0.798	0.682	0.366	0.322	0.299	0.288	0.503	0.835
0.25	0.318	0.383	0.486	0.551	0.620	0.700	0.912	0.875	0.754	0.418	0.362	0.336	0.318	0.560	0.912
0.30	0.349	0.419	0.552	0.614	0.681	0.768	0.993	0.954	0.824	0.469	0.400	0.376	0.349	0.617	0.993
0.40	0.415	0.508	0.678	0.749	0.837	0.912	1.155	1.130	0.979	0.593	0.486	0.463	0.415	0.742	1.155
0.50	0.488	0.609	0.821	0.905	1.009	1.074	1.342	1.335	1.164	0.732	0.593	0.566	0.488	0.887	1.342
0.60	0.578	0.716	0.985	1.102	1.212	1.274	1.568	1.589	1.378	0.897	0.732	0.696	0.578	1.061	1.589
0.70	0.689	0.859	1.191	1.363	1.454	1.545	1.893	1.942	1.674	1.122	0.910	0.859	0.689	1.292	1.942
0.80	0.845	1.052	1.481	1.713	1.813	1.960	2.364	2.437	2.130	1.469	1.165	1.086	0.845	1.626	2.437
0.85	0.959	1.188	1.688	1.975	2.077	2.262	2.719	2.828	2.461	1.740	1.343	1.254	0.959	1.875	2.828
0.90	1.122	1.391	1.989	2.371	2.466	2.741	3.221	3.378	2.954	2.117	1.587	1.482	1.122	2.235	3.378
0.91	1.174	1.438	2.098	2.454	2.564	2.877	3.337	3.535	3.077	2.201	1.650	1.542	1.174	2.329	3.535
0.92	1.225	1.502	2.194	2.582	2.654	3.017	3.525	3.694	3.215	2.328	1.726	1.620	1.225	2.440	3.694
0.93	1.285	1.583	2.309	2.703	2.797	3.197	3.689	3.892	3.382	2.452	1.803	1.684	1.285	2.565	3.892
0.94	1.351	1.671	2.436	2.839	2.940	3.366	3.897	4.130	3.600	2.613	1.916	1.766	1.351	2.710	4.130
0.95	1.444	1.752	2.591	2.991	3.092	3.599	4.153	4.360	3.842	2.748	2.009	1.888	1.444	2.872	4.360
0.96	1.566	1.872	2.795	3.189	3.322	3.901	4.468	4.655	4.238	2.951	2.139	2.017	1.566	3.093	4.655
0.97	1.740	1.999	3.041	3.456	3.609	4.239	4.849	5.075	4.643	3.223	2.307	2.217	1.740	3.367	5.075
0.98	1.960	2.206	3.379	3.810	3.976	4.678	5.305	5.737	5.242	3.602	2.615	2.425	1.960	3.745	5.737
0.99	2.317	2.574	4.052	4.389	4.681	5.499	6.367	6.777	6.500	4.228	3.038	2.823	2.317	4.437	6.777
0.995	2.811	2.907	4.534	4.878	5.265	6.314	7.427	7.974	7.970	4.903	3.666	3.318	2.811	5.164	7.974
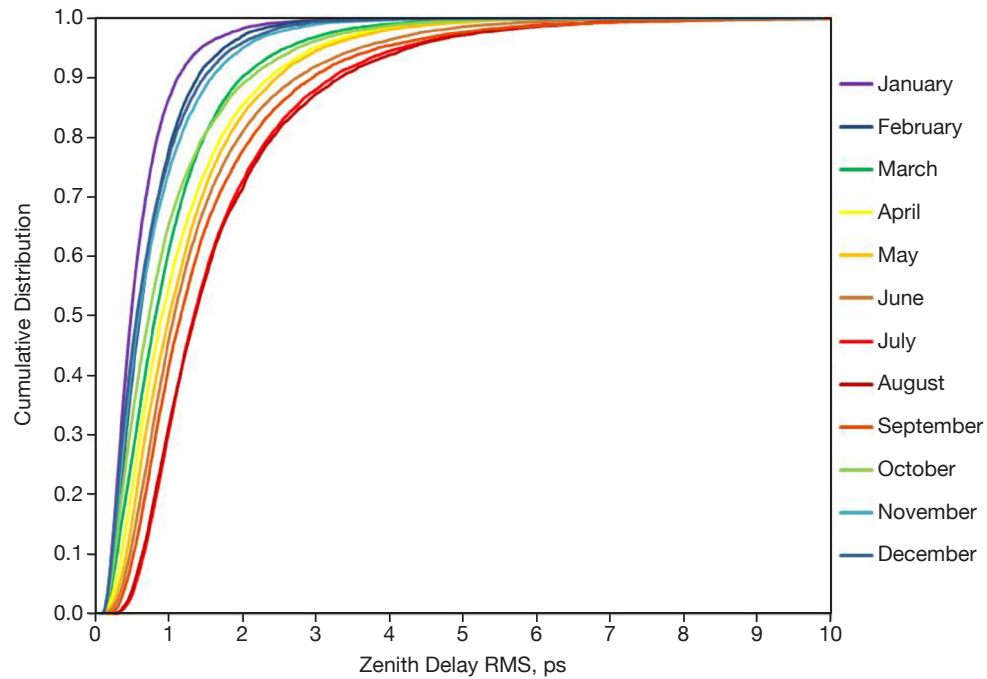
Figure 1. Goldstone monthly cumulative distribution curves of zenith delay RMS for the east–west Apollo STI baseline.
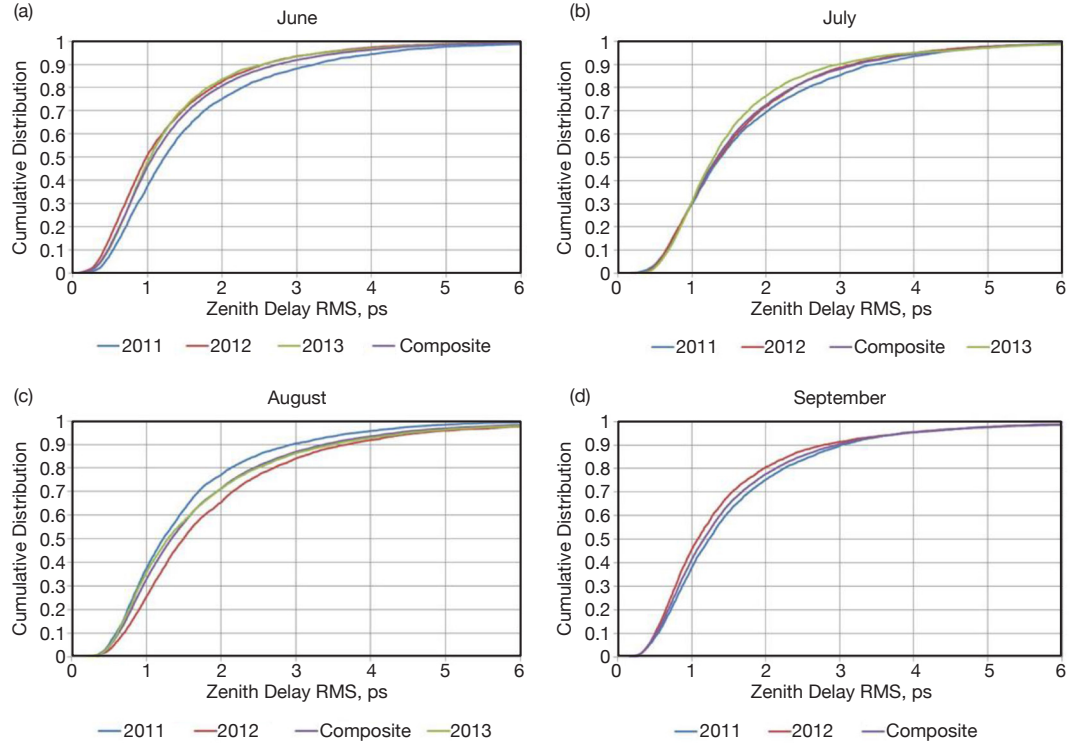
Figure 2. Goldstone zenith delay RMS CD curves for the warm summer months from individual years, including the yearly composite CD curve.

Figure 3 displays the CD curves for the zenith delay RMS for the cool (mostly winter) months at Goldstone. The spread between the individual year CDs and the composite is very small for November and January and larger for December and February, especially at the higher CD values. The 90 percent values of the composite CD curves for the winter months lie in between 1.1 ps and 1.6 ps.

Figure 4 displays the CD curves of zenith delay RMS for intermediate autumn and spring months as well as the composite CD curve for each month. These CD curves lie in between those of the warmer months (Figure 2) and the cooler months (Figure 3). The spread between CD curves for the given month at different years is very small for May and October and somewhat larger for March and April. The 90 percent values of the composite CD curves for these intermediate months lie in between 2.0 and 2.5 ps.

Expected Array Loss Statistics for Selected Configurations

The delay RMS values presented in the previous section were converted to values of expected array loss using the procedure outlined in Section II. Tables 3, 4, 5, and 6 display the monthly, minimum, average, and maximum yearly expected array loss dB values for selected combinations of arrayed Goldstone antennas referenced to 7.15 GHz (X-band) at a 20-deg elevation angle for CD values ranging from 0 percent to 99.5 percent. The yearly average of array loss at 90 percent for a 20-deg elevation angle appear to run ~0.05 dB to ~0.2 dB, consistent with expected upper limits inferred from uplink array demo results at X-band (see Section III.C) [14–16]. For the two station array configurations, the dB values for a given CD and month are lowest for the two DSN antennas (DSS-24/DSS-25 in Table 4) with the shortest separation as expected.
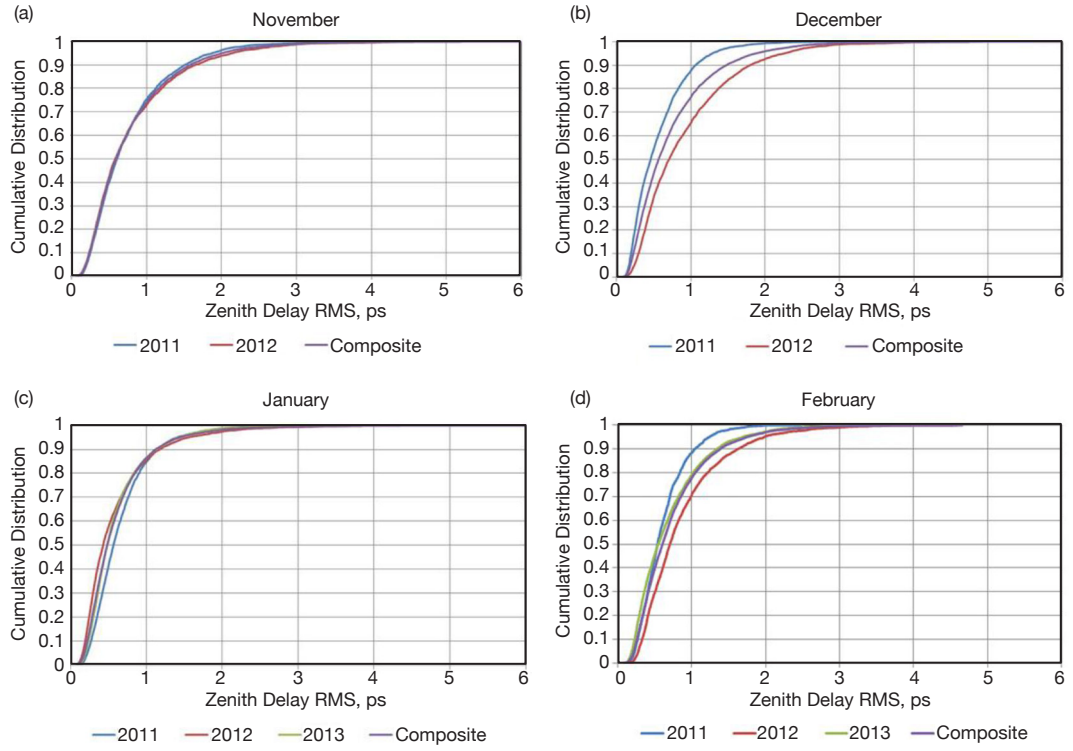
Figure 3. Goldstone zenith delay RMS CD curves for the cooler months from individual years, including the yearly composite CD curve for that month.
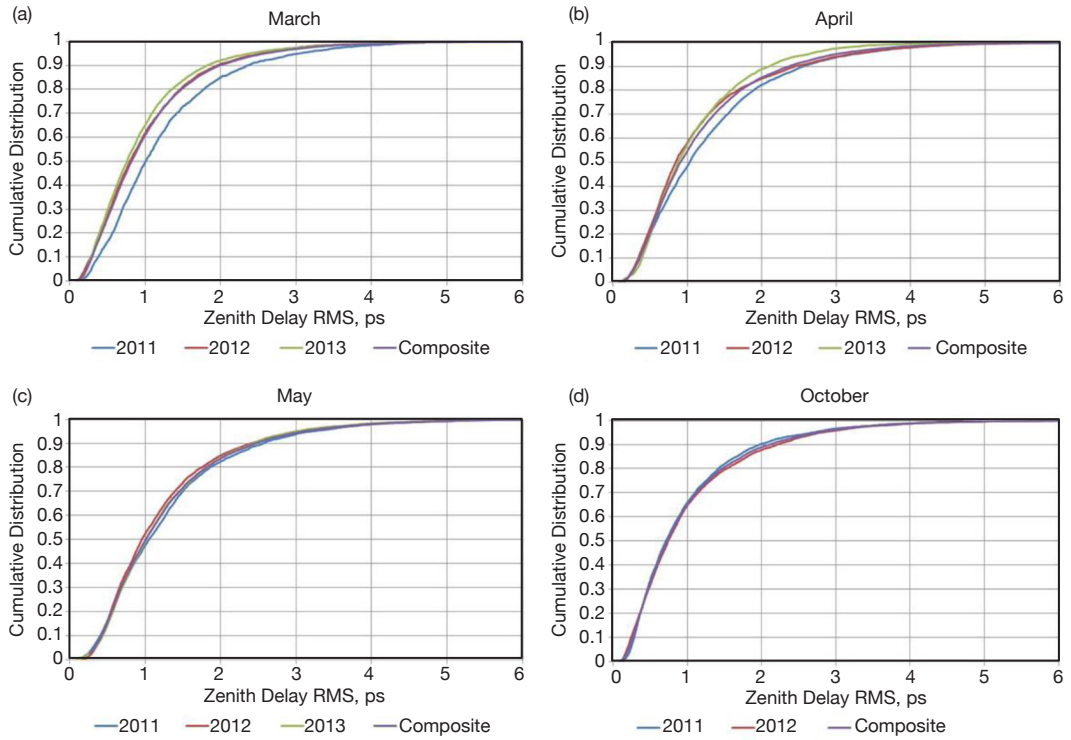
Figure 4. Goldstone zenith delay RMS CD curves for the intermediate spring and autumn months from individual years, including the yearly composite CD curve for that month.

Table 3. DSS-24/25/26 expected array loss at 7.15 GHz, 20-deg elevation angle.

CD	Jan	Feb	Mar	Apr	May	Jun	Jul	Aug	Sep	Oct	Nov	Dec	Year Min	Year Avg	Year Max
0.00	0.000	0.000	0.000	0.000	0.000	0.000	0.001	0.001	0.001	0.000	0.000	0.000	0.000	0.000	0.001
0.10	0.001	0.002	0.002	0.003	0.004	0.005	0.011	0.010	0.007	0.002	0.001	0.001	0.001	0.004	0.011
0.20	0.002	0.003	0.004	0.006	0.008	0.010	0.017	0.016	0.011	0.003	0.003	0.002	0.002	0.006	0.017
0.25	0.003	0.004	0.006	0.007	0.009	0.012	0.021	0.019	0.014	0.004	0.003	0.003	0.003	0.008	0.021
0.30	0.003	0.004	0.008	0.009	0.011	0.015	0.024	0.022	0.017	0.005	0.004	0.003	0.003	0.009	0.024
0.40	0.004	0.006	0.011	0.014	0.017	0.020	0.033	0.031	0.024	0.009	0.006	0.005	0.004	0.014	0.033
0.50	0.006	0.009	0.017	0.020	0.025	0.028	0.044	0.044	0.033	0.013	0.009	0.008	0.006	0.019	0.044
0.60	0.008	0.013	0.024	0.030	0.036	0.040	0.060	0.062	0.047	0.020	0.013	0.012	0.008	0.028	0.062
0.70	0.012	0.018	0.035	0.046	0.052	0.059	0.088	0.092	0.069	0.031	0.020	0.018	0.012	0.041	0.092
0.80	0.018	0.027	0.054	0.072	0.080	0.094	0.136	0.145	0.111	0.053	0.033	0.029	0.018	0.065	0.145
0.85	0.023	0.035	0.070	0.095	0.105	0.125	0.179	0.194	0.147	0.074	0.044	0.039	0.023	0.086	0.194
0.90	0.031	0.048	0.097	0.137	0.148	0.182	0.250	0.274	0.211	0.109	0.062	0.054	0.031	0.122	0.274
0.91	0.034	0.051	0.108	0.147	0.160	0.200	0.268	0.299	0.229	0.118	0.067	0.058	0.034	0.132	0.299
0.92	0.037	0.055	0.117	0.162	0.171	0.220	0.298	0.326	0.249	0.132	0.073	0.064	0.037	0.145	0.326
0.93	0.041	0.062	0.130	0.177	0.190	0.246	0.325	0.361	0.275	0.146	0.080	0.070	0.041	0.160	0.361
0.94	0.045	0.069	0.145	0.195	0.209	0.272	0.361	0.404	0.310	0.166	0.090	0.076	0.045	0.178	0.404
0.95	0.051	0.075	0.163	0.216	0.231	0.310	0.408	0.448	0.352	0.183	0.099	0.087	0.051	0.200	0.448
0.96	0.060	0.086	0.189	0.245	0.265	0.362	0.470	0.507	0.424	0.211	0.112	0.099	0.060	0.231	0.507
0.97	0.074	0.098	0.223	0.287	0.312	0.425	0.548	0.597	0.505	0.250	0.130	0.120	0.074	0.272	0.597
0.98	0.094	0.119	0.274	0.346	0.376	0.512	0.649	0.750	0.634	0.311	0.166	0.143	0.094	0.335	0.750
0.99	0.131	0.161	0.390	0.454	0.513	0.693	0.906	1.013	0.941	0.423	0.223	0.193	0.131	0.463	1.013
0.995	0.191	0.205	0.483	0.554	0.640	0.893	1.190	1.344	1.342	0.560	0.321	0.265	0.191	0.617	1.344

Table 4. DSS-24/25 expected array loss at 7.15 GHz, 20-deg elevation angle.

CD	Jan	Feb	Mar	Apr	May	Jun	Jul	Aug	Sep	Oct	Nov	Dec	Year Min	Year Avg	Year Max
0.00	0.000	0.000	0.000	0.000	0.000	0.000	0.000	0.000	0.000	0.000	0.000	0.000	0.000	0.000	0.000
0.10	0.001	0.001	0.001	0.001	0.002	0.002	0.005	0.004	0.003	0.001	0.001	0.001	0.001	0.002	0.005
0.20	0.001	0.001	0.002	0.003	0.003	0.004	0.007	0.007	0.005	0.001	0.001	0.001	0.001	0.003	0.007
0.25	0.001	0.002	0.003	0.003	0.004	0.005	0.009	0.008	0.006	0.002	0.001	0.001	0.001	0.003	0.009
0.30	0.001	0.002	0.003	0.004	0.005	0.006	0.010	0.010	0.007	0.002	0.002	0.002	0.001	0.004	0.010
0.40	0.002	0.003	0.005	0.006	0.007	0.009	0.014	0.014	0.010	0.004	0.003	0.002	0.002	0.006	0.014
0.50	0.003	0.004	0.007	0.009	0.011	0.012	0.019	0.019	0.014	0.006	0.004	0.003	0.003	0.008	0.019
0.60	0.004	0.005	0.010	0.013	0.016	0.017	0.026	0.027	0.020	0.009	0.006	0.005	0.004	0.012	0.027
0.70	0.005	0.008	0.015	0.020	0.022	0.025	0.038	0.040	0.030	0.013	0.009	0.008	0.005	0.018	0.040
0.80	0.008	0.012	0.023	0.031	0.035	0.041	0.059	0.063	0.048	0.023	0.014	0.012	0.008	0.028	0.063
0.85	0.010	0.015	0.030	0.041	0.045	0.054	0.078	0.084	0.064	0.032	0.019	0.017	0.010	0.037	0.084
0.90	0.013	0.020	0.042	0.059	0.064	0.079	0.109	0.119	0.092	0.047	0.027	0.023	0.013	0.053	0.119
0.91	0.015	0.022	0.046	0.063	0.069	0.087	0.116	0.130	0.099	0.051	0.029	0.025	0.015	0.057	0.130
0.92	0.016	0.024	0.051	0.070	0.074	0.095	0.130	0.142	0.108	0.057	0.031	0.028	0.016	0.063	0.142
0.93	0.017	0.026	0.056	0.077	0.082	0.107	0.142	0.158	0.120	0.063	0.034	0.030	0.017	0.069	0.158
0.94	0.019	0.030	0.062	0.085	0.091	0.118	0.158	0.177	0.135	0.072	0.039	0.033	0.019	0.077	0.177
0.95	0.022	0.032	0.071	0.094	0.100	0.135	0.179	0.197	0.154	0.079	0.043	0.038	0.022	0.087	0.197
0.96	0.026	0.037	0.082	0.107	0.115	0.158	0.207	0.224	0.186	0.091	0.048	0.043	0.026	0.100	0.224
0.97	0.032	0.042	0.097	0.125	0.136	0.186	0.242	0.265	0.223	0.109	0.056	0.052	0.032	0.119	0.265
0.98	0.041	0.051	0.119	0.151	0.164	0.226	0.288	0.335	0.282	0.135	0.072	0.062	0.041	0.146	0.335
0.99	0.057	0.070	0.171	0.199	0.226	0.309	0.409	0.460	0.425	0.185	0.097	0.084	0.057	0.204	0.460
0.995	0.083	0.089	0.212	0.245	0.284	0.402	0.546	0.622	0.621	0.247	0.140	0.115	0.083	0.274	0.622

Table 5. DSS-24/26 expected array loss at 7.15 GHz, 20-deg elevation angle.

CD	Jan	Feb	Mar	Apr	May	Jun	Jul	Aug	Sep	Oct	Nov	Dec	Year Min	Year Avg	Year Max
0.00	0.000	0.000	0.000	0.000	0.000	0.000	0.001	0.001	0.001	0.000	0.000	0.000	0.000	0.000	0.001
0.10	0.002	0.002	0.003	0.004	0.006	0.007	0.014	0.012	0.008	0.002	0.002	0.002	0.002	0.005	0.014
0.20	0.003	0.004	0.006	0.008	0.010	0.012	0.022	0.020	0.014	0.004	0.003	0.003	0.003	0.008	0.022
0.25	0.003	0.005	0.007	0.009	0.012	0.015	0.026	0.024	0.018	0.005	0.004	0.004	0.003	0.010	0.026
0.30	0.004	0.005	0.010	0.012	0.014	0.018	0.031	0.028	0.021	0.007	0.005	0.004	0.004	0.012	0.031
0.40	0.005	0.008	0.014	0.017	0.022	0.026	0.041	0.040	0.030	0.011	0.007	0.007	0.005	0.017	0.041
0.50	0.007	0.012	0.021	0.025	0.032	0.036	0.056	0.055	0.042	0.017	0.011	0.010	0.007	0.024	0.056
0.60	0.010	0.016	0.030	0.038	0.046	0.050	0.076	0.078	0.059	0.025	0.017	0.015	0.010	0.035	0.078
0.70	0.015	0.023	0.044	0.058	0.065	0.074	0.110	0.116	0.087	0.039	0.026	0.023	0.015	0.052	0.116
0.80	0.022	0.034	0.068	0.091	0.101	0.118	0.171	0.181	0.139	0.067	0.042	0.037	0.022	0.082	0.181
0.85	0.029	0.044	0.088	0.120	0.133	0.157	0.225	0.243	0.185	0.094	0.056	0.049	0.029	0.108	0.243
0.90	0.039	0.060	0.122	0.172	0.186	0.228	0.312	0.342	0.264	0.138	0.078	0.068	0.039	0.153	0.342
0.91	0.043	0.064	0.135	0.184	0.200	0.251	0.334	0.373	0.286	0.149	0.084	0.074	0.043	0.166	0.373
0.92	0.047	0.070	0.148	0.203	0.214	0.275	0.371	0.405	0.311	0.166	0.092	0.081	0.047	0.182	0.405
0.93	0.051	0.078	0.163	0.222	0.237	0.307	0.404	0.447	0.342	0.184	0.100	0.088	0.051	0.201	0.447
0.94	0.057	0.086	0.181	0.244	0.261	0.339	0.448	0.500	0.386	0.208	0.113	0.096	0.057	0.223	0.500
0.95	0.065	0.095	0.205	0.270	0.288	0.386	0.505	0.553	0.437	0.229	0.124	0.110	0.065	0.250	0.553
0.96	0.076	0.108	0.237	0.306	0.331	0.449	0.579	0.624	0.525	0.263	0.141	0.125	0.076	0.288	0.624
0.97	0.094	0.123	0.279	0.357	0.388	0.525	0.672	0.730	0.621	0.312	0.163	0.151	0.094	0.339	0.730
0.98	0.118	0.149	0.342	0.430	0.466	0.630	0.790	0.907	0.774	0.386	0.208	0.180	0.118	0.416	0.907
0.99	0.164	0.202	0.482	0.560	0.631	0.842	1.084	1.201	1.122	0.522	0.279	0.242	0.164	0.571	1.201
0.995	0.240	0.256	0.595	0.680	0.780	1.069	1.389	1.547	1.545	0.686	0.399	0.330	0.240	0.753	1.547

Table 6. DSS-25/26 expected array loss at 7.15 GHz, 20-deg elevation angle.

CD	Jan	Feb	Mar	Apr	May	Jun	Jul	Aug	Sep	Oct	Nov	Dec	Year Min	Year Avg	Year Max
0.00	0.000	0.000	0.000	0.000	0.000	0.000	0.000	0.001	0.000	0.000	0.000	0.000	0.000	0.000	0.001
0.10	0.001	0.001	0.001	0.002	0.002	0.003	0.006	0.005	0.004	0.001	0.001	0.001	0.001	0.002	0.006
0.20	0.001	0.002	0.002	0.003	0.004	0.005	0.010	0.009	0.006	0.002	0.001	0.001	0.001	0.003	0.010
0.25	0.001	0.002	0.003	0.004	0.005	0.007	0.011	0.011	0.008	0.002	0.002	0.002	0.001	0.004	0.011
0.30	0.002	0.002	0.004	0.005	0.006	0.008	0.014	0.013	0.009	0.003	0.002	0.002	0.002	0.005	0.014
0.40	0.002	0.004	0.006	0.008	0.010	0.011	0.018	0.018	0.013	0.005	0.003	0.003	0.002	0.008	0.018
0.50	0.003	0.005	0.009	0.011	0.014	0.016	0.025	0.024	0.019	0.007	0.005	0.004	0.003	0.011	0.025
0.60	0.005	0.007	0.013	0.017	0.020	0.022	0.034	0.035	0.026	0.011	0.007	0.007	0.005	0.015	0.035
0.70	0.007	0.010	0.019	0.025	0.029	0.033	0.049	0.052	0.038	0.017	0.011	0.010	0.007	0.023	0.052
0.80	0.010	0.015	0.030	0.040	0.045	0.052	0.076	0.081	0.062	0.030	0.019	0.016	0.010	0.036	0.081
0.85	0.013	0.019	0.039	0.053	0.059	0.070	0.100	0.109	0.082	0.041	0.025	0.022	0.013	0.048	0.109
0.90	0.017	0.027	0.054	0.077	0.083	0.102	0.140	0.154	0.118	0.061	0.035	0.030	0.017	0.068	0.154
0.91	0.019	0.028	0.060	0.082	0.089	0.112	0.150	0.168	0.128	0.066	0.037	0.033	0.019	0.074	0.168
0.92	0.021	0.031	0.066	0.091	0.096	0.123	0.167	0.184	0.140	0.074	0.041	0.036	0.021	0.081	0.184
0.93	0.023	0.034	0.073	0.099	0.106	0.138	0.183	0.203	0.154	0.082	0.044	0.039	0.023	0.089	0.203
0.94	0.025	0.038	0.081	0.109	0.117	0.153	0.204	0.228	0.175	0.093	0.050	0.043	0.025	0.100	0.228
0.95	0.029	0.042	0.091	0.121	0.129	0.174	0.231	0.253	0.198	0.103	0.055	0.049	0.029	0.112	0.253
0.96	0.034	0.048	0.106	0.138	0.149	0.204	0.266	0.288	0.240	0.118	0.062	0.056	0.034	0.130	0.288
0.97	0.041	0.055	0.125	0.161	0.175	0.240	0.311	0.340	0.286	0.140	0.073	0.067	0.041	0.153	0.340
0.98	0.053	0.066	0.154	0.195	0.212	0.290	0.370	0.429	0.361	0.175	0.093	0.080	0.053	0.189	0.429
0.99	0.073	0.090	0.220	0.257	0.291	0.396	0.522	0.586	0.542	0.239	0.125	0.108	0.073	0.262	0.586
0.995	0.107	0.115	0.273	0.315	0.364	0.514	0.693	0.787	0.786	0.318	0.181	0.149	0.107	0.351	0.787

Table 7 displays the expected loss for given CD values for an array consisting of DSS-25 and DSS-26 at 34.5 GHz (Ka-band) using the method outlined in Section II. The expected array loss at a CD of 90 percent is typically below 1 dB for the winter months but reaches ~2 dB during the summer months. The 34.5-GHz frequency uplink capability is used for radio science carrier-only experiments and is currently only available at DSS-25. Both DSS-25 and DSS-26 are Ka-band downlink-capable antennas at 32 GHz; thus, such statistics can be used to infer array loss for downlink scenarios involving these two antennas when the received signal is too weak to allow real-time phase compensation of atmospheric effects.

Table 7. DSS-25/26 expected array loss at 34.5 GHz, 20-deg elevation angle.

CD	Jan	Feb	Mar	Apr	May	Jun	Jul	Aug	Sep	Oct	Nov	Dec	Year Min	Year Avg	Year Max
0.00	0.002	0.003	0.002	0.002	0.003	0.003	0.009	0.014	0.008	0.002	0.001	0.002	0.001	0.004	0.014
0.10	0.016	0.022	0.027	0.040	0.055	0.069	0.133	0.121	0.083	0.022	0.018	0.016	0.016	0.045	0.133
0.20	0.026	0.037	0.055	0.074	0.096	0.120	0.211	0.194	0.142	0.041	0.032	0.028	0.026	0.078	0.211
0.25	0.031	0.045	0.073	0.093	0.118	0.150	0.251	0.231	0.173	0.054	0.041	0.035	0.031	0.096	0.251
0.30	0.038	0.054	0.094	0.116	0.142	0.179	0.296	0.274	0.206	0.068	0.049	0.044	0.038	0.117	0.296
0.40	0.053	0.079	0.140	0.171	0.212	0.251	0.395	0.379	0.288	0.108	0.073	0.066	0.053	0.168	0.395
0.50	0.073	0.114	0.204	0.247	0.305	0.344	0.524	0.519	0.401	0.164	0.108	0.099	0.073	0.237	0.524
0.60	0.102	0.156	0.291	0.361	0.433	0.476	0.698	0.714	0.550	0.243	0.163	0.148	0.102	0.336	0.714
0.70	0.145	0.223	0.419	0.539	0.607	0.679	0.973	1.016	0.785	0.374	0.250	0.223	0.145	0.488	1.016
0.80	0.216	0.331	0.629	0.818	0.902	1.032	1.399	1.465	1.185	0.619	0.402	0.351	0.216	0.745	1.465
0.85	0.277	0.417	0.796	1.046	1.137	1.306	1.717	1.811	1.487	0.840	0.525	0.462	0.277	0.957	1.811
0.90	0.374	0.560	1.058	1.405	1.491	1.736	2.124	2.236	1.916	1.173	0.713	0.629	0.374	1.281	2.236
0.91	0.407	0.596	1.156	1.481	1.580	1.852	2.207	2.339	2.014	1.250	0.765	0.676	0.407	1.367	2.339
0.92	0.441	0.645	1.243	1.596	1.659	1.966	2.333	2.434	2.119	1.366	0.829	0.739	0.441	1.468	2.434
0.93	0.483	0.709	1.349	1.703	1.784	2.106	2.432	2.540	2.238	1.479	0.894	0.793	0.483	1.580	2.540
0.94	0.531	0.782	1.465	1.820	1.904	2.228	2.543	2.648	2.379	1.623	0.993	0.862	0.531	1.709	2.648
0.95	0.600	0.851	1.604	1.945	2.026	2.378	2.657	2.734	2.515	1.742	1.076	0.968	0.600	1.848	2.734
0.96	0.696	0.954	1.782	2.100	2.197	2.545	2.768	2.819	2.690	1.913	1.194	1.083	0.696	2.027	2.819
0.97	0.840	1.067	1.986	2.288	2.385	2.691	2.863	2.903	2.816	2.125	1.346	1.265	0.840	2.228	2.903
0.98	1.032	1.254	2.237	2.498	2.581	2.825	2.934	2.971	2.926	2.381	1.625	1.454	1.032	2.463	2.971
0.99	1.356	1.589	2.615	2.743	2.826	2.953	2.997	3.004	3.000	2.687	1.983	1.806	1.356	2.759	3.004
0.995	1.796	1.877	2.787	2.869	2.929	2.996	3.009	3.010	3.010	2.873	2.419	2.194	1.796	2.916	3.010

Examination of Equation (1) shows that the expected value of loss cannot exceed $-10\log(1/N)$, or 3 dB for $N = 2$ and 4.8 dB for $N = 3$. Table 7 shows that this limit is reached about 1 percent of the time at 34.5 GHz during summer months in Goldstone. Values in the tables that approach the limit should be interpreted cautiously because sometimes the instantaneous loss will greatly exceed the expected value. Values well below the limit can be taken as representative.

B. Canberra Complex

Delay RMS Statistics

The monthly and yearly zenith delay RMS statistics are presented in Table 8 for the Canberra DSN site as extracted from the east–west STI baseline data. June appears to be the month with the lowest delay RMS of ~0.109 ps, comparable to the expected ~0.1 ps level of instrumental noise. December has the highest delay RMS at about 13.348 ps. The 90 percent year average is about 4.12 ps (compare this to the Goldstone 90 percent yearly value of 2.24 ps), consistent with the wetter climate at Canberra. We shall see how these values translate to dB expected array loss values for different frequency bands, elevation angles,

Table 8. Zenith delay RMS in ps, Canberra, 250-m baseline.

CD	Jan	Feb	Mar	Apr	May	Jun	Jul	Aug	Sep	Oct	Nov	Dec	Year Min	Year Avg	Year Max
0.00	0.178	0.280	0.224	0.177	0.118	0.109	0.120	0.378	0.160	0.132	0.157	0.255	0.109	0.191	0.378
0.10	0.826	0.795	0.711	0.546	0.441	0.474	0.471	0.496	0.609	0.525	0.731	0.785	0.441	0.617	0.826
0.20	1.104	1.001	0.975	0.732	0.598	0.638	0.641	0.731	0.861	0.733	0.961	1.012	0.598	0.832	1.104
0.25	1.244	1.105	1.109	0.830	0.671	0.721	0.728	0.859	0.971	0.836	1.082	1.117	0.671	0.940	1.244
0.30	1.370	1.195	1.241	0.923	0.741	0.796	0.816	0.996	1.080	0.944	1.208	1.222	0.741	1.044	1.370
0.40	1.647	1.405	1.509	1.136	0.904	0.954	1.013	1.286	1.332	1.201	1.480	1.463	0.904	1.278	1.647
0.50	1.976	1.641	1.819	1.386	1.110	1.147	1.262	1.611	1.589	1.452	1.788	1.762	1.110	1.545	1.976
0.60	2.396	1.959	2.195	1.719	1.352	1.419	1.569	1.966	1.897	1.797	2.149	2.148	1.352	1.881	2.396
0.70	2.946	2.365	2.715	2.149	1.663	1.758	2.001	2.355	2.282	2.252	2.617	2.675	1.663	2.315	2.946
0.80	3.730	3.005	3.418	2.741	2.189	2.233	2.631	2.944	2.831	2.879	3.396	3.638	2.189	2.970	3.730
0.85	4.329	3.485	3.931	3.153	2.575	2.546	3.039	3.366	3.254	3.358	3.979	4.300	2.546	3.443	4.329
0.90	5.168	4.173	4.750	3.807	3.061	2.975	3.611	3.894	3.818	3.968	4.883	5.377	2.975	4.124	5.377
0.91	5.393	4.358	4.954	3.985	3.182	3.078	3.750	4.034	3.959	4.139	5.105	5.727	3.078	4.305	5.727
0.92	5.644	4.587	5.184	4.136	3.300	3.225	3.913	4.203	4.103	4.305	5.399	5.989	3.225	4.499	5.989
0.93	5.928	4.817	5.450	4.357	3.483	3.378	4.087	4.381	4.330	4.505	5.706	6.343	3.378	4.730	6.343
0.94	6.248	5.067	5.783	4.549	3.640	3.554	4.263	4.598	4.514	4.738	6.126	6.737	3.554	4.985	6.737
0.95	6.585	5.428	6.131	4.845	3.862	3.769	4.509	4.860	4.791	5.028	6.636	7.106	3.769	5.296	7.106
0.96	7.126	5.828	6.585	5.197	4.159	4.081	4.755	5.167	5.061	5.344	7.124	7.695	4.081	5.677	7.695
0.97	7.704	6.359	7.159	5.638	4.490	4.424	5.116	5.565	5.387	5.788	7.890	8.435	4.424	6.163	8.435
0.98	8.772	7.298	8.070	6.286	5.105	4.992	5.539	6.152	5.896	6.631	8.760	9.596	4.992	6.925	9.596
0.99	10.538	8.903	9.027	7.268	6.328	6.237	6.474	6.872	7.041	7.730	10.302	11.292	6.237	8.168	11.292
0.995	12.341	9.974	10.637	8.758	7.356	7.070	7.254	7.728	8.237	8.900	12.126	13.348	7.070	9.477	13.348

and array configurations later. (Note that the Canberra site is in the southern hemisphere and Goldstone is in the northern hemisphere.)

Figure 5 displays the monthly CD curves for the zenith delay RMS extracted from the east–west STI baseline data for Canberra. Note that from Figure 5 there is a seasonal separation between the CD curves, although not as strong as that for Goldstone (see Figure 1). The summer curves for Canberra tend to lie on the right side of Figure 5, the winter month CD curves tend to lie on the left side, and the autumn/spring CD curves tend to lie in between. The summer month CD curves are shown in bluish colors, the winter month curves are shown in reddish colors, and the intermediate spring and autumn curves are shown in green-yellow colors.

Figure 6 displays the CDs of zenith delay RMS for the warm summer months. There is a reasonable degree of consistency between the individual year CDs and the composite CD for each month, with the spread being much less for November, January, and February and a little more for December. It should be noted that the December 2011 CD curve is based on a partial month of data: about 42 percent due to outages caused by various equipment and operational issues. The CD curves for most other months are based on almost complete months of data.

Figure 7 displays the CD curves for the zenith delay RMS for the cool winter months. The spread between the individual year CDs and the composite is very small for July and somewhat larger for May, June, and August.

Figure 8 displays the CD curves of zenith delay RMS for selected intermediate autumn and spring months as well as the composite CD for each month. The spread for curves of the same months in different years is very small for March and April and somewhat larger for September and October.
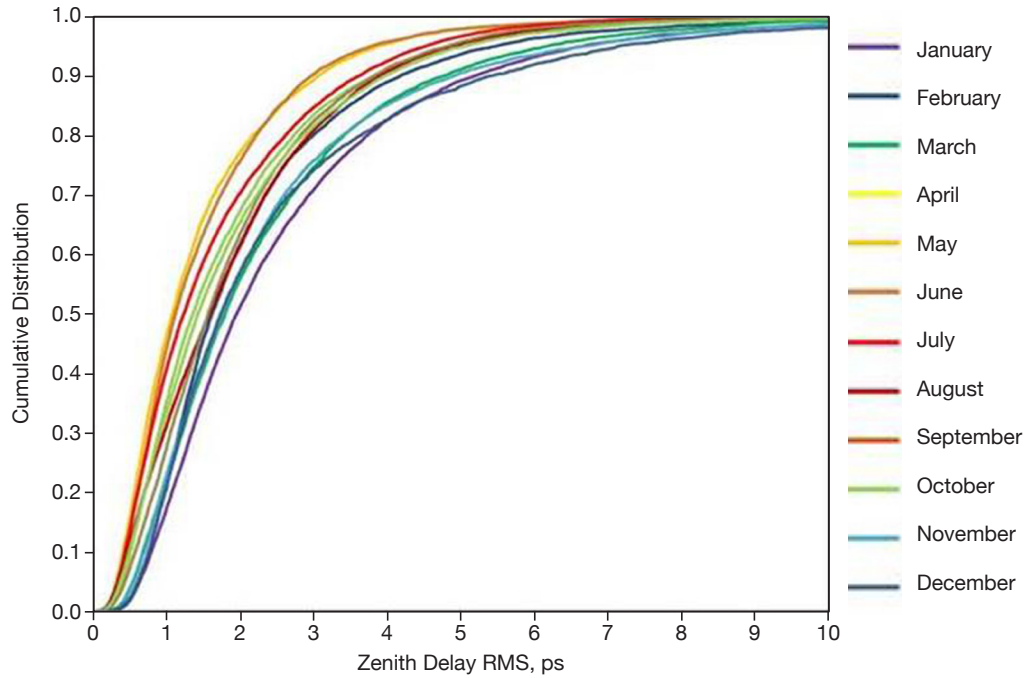
Figure 5. Monthly cumulative distribution curves of zenith delay RMS for the Canberra east–west STI baseline.
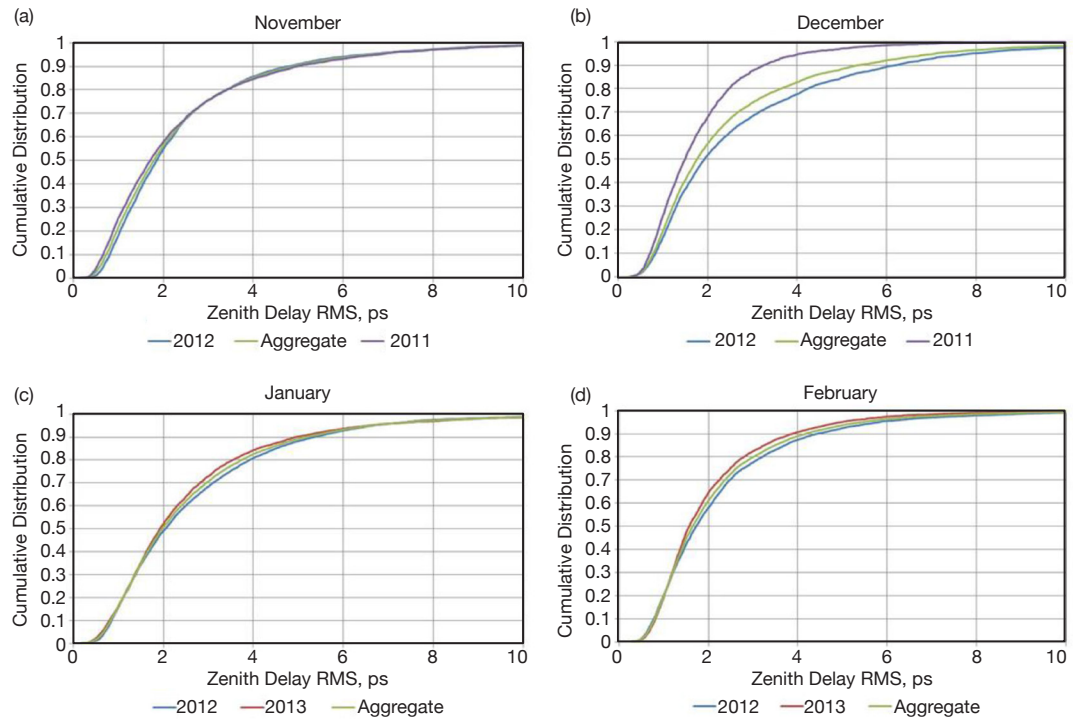
Figure 6. Canberra zenith delay RMS CD curves for the warm summer months from individual years, including the yearly composite CD curve.
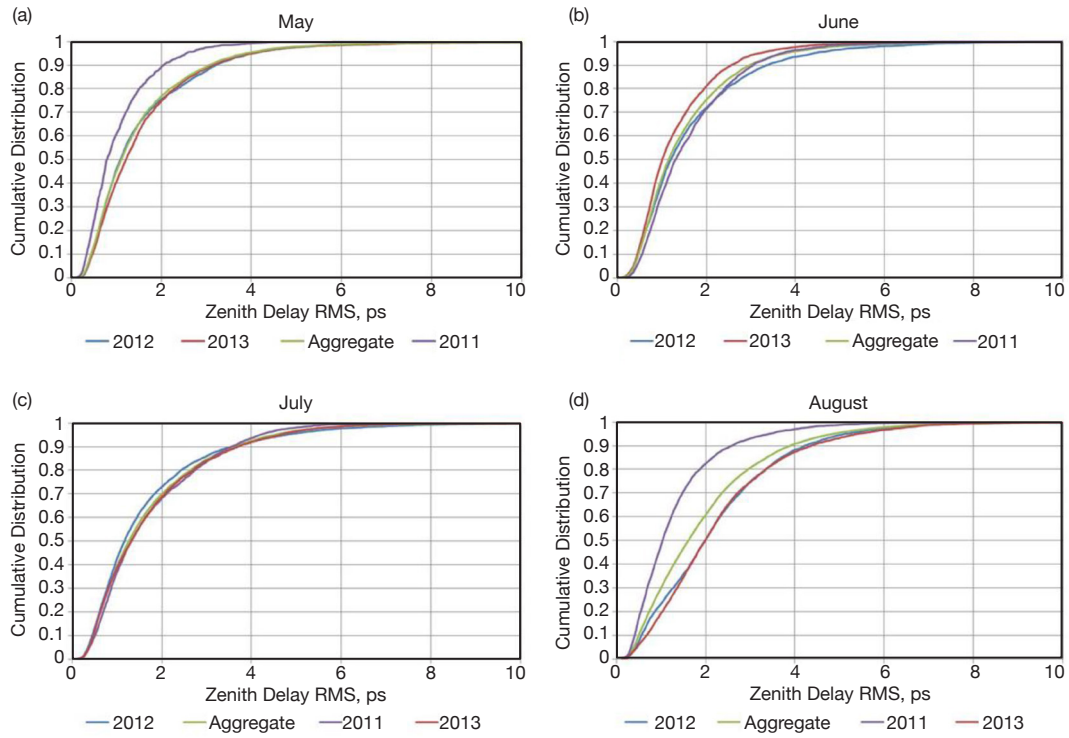
Figure 7. Canberra zenith delay RMS CD curves for the cooler winter months from individual years, including the yearly composite CD curve.
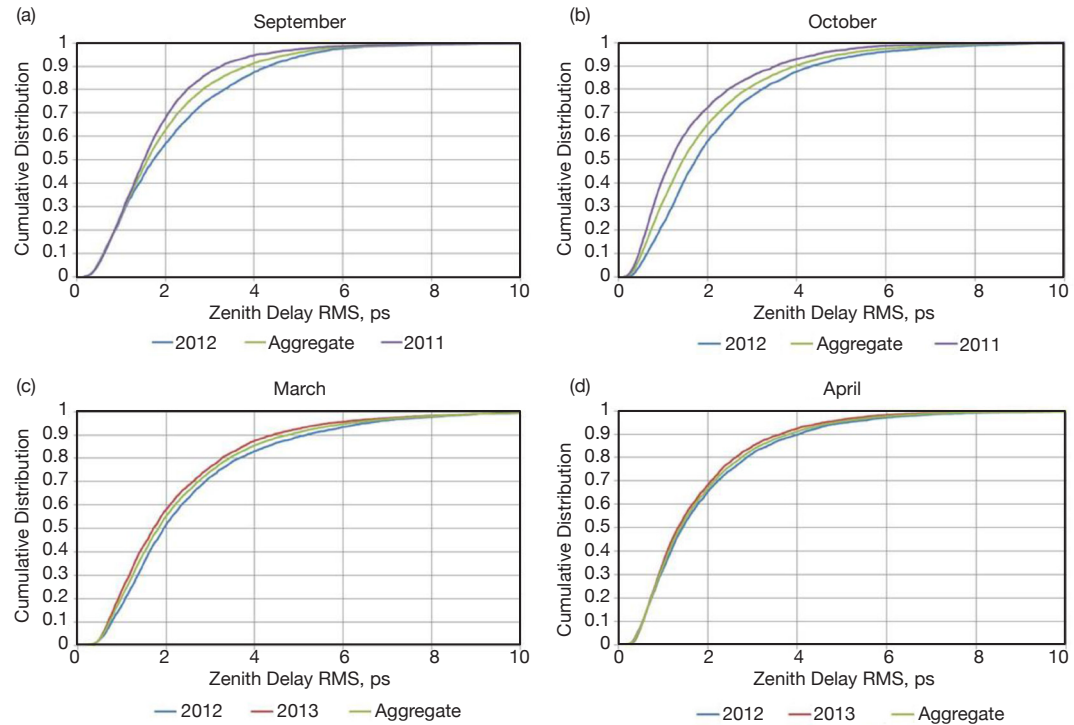
Figure 8. Canberra zenith delay RMS CD curves for the intermediate spring and autumn months from individual years, including the yearly composite CD curve.

Expected Array Loss Statistics for Selected Configurations

The delay RMS values presented in the previous section were converted to values of expected array loss for selected existing antenna configurations using the procedure outlined in Section II. Tables 9, 10, 11, and 12 display the monthly, yearly, and minimum and maximum monthly array loss dB values for selected array configurations of existing DSN antennas at the Canberra complex referenced to X-band at a 20-deg elevation angle.

The X-band yearly average of expected array loss values at 90 percent for 20 deg elevation appear to run on order of 0.14 dB to 0.4 dB for the DSS-34/35/36 array, which is greater than the corresponding range for Goldstone's DSS-24/25/26 array (0.03 to 0.27 dB in Table 3), consistent with Canberra's generally wetter climate. For the two-station array configurations, the dB values for a given CD and month are lowest for the two DSN antennas (DSS-35/DSS-36 in Table 12) with the shortest separation.

Table 13 displays the monthly, yearly, and minimum and maximum monthly expected array loss dB values for the array configuration consisting of DSS-34 and DSS-35 referenced to Ka-band uplink frequency of 34.5 GHz at a 20-deg elevation angle. It is emphasized that neither of these stations currently have operational uplink capability at Ka-band. Note that the maximum 3 dB limit of the average method is obtained for every single month at the 99.5 percent CD and lies very close to it for CD values above 95 percent for all months. It can be seen that the expected value of the loss reaches its maximum of 3 dB nearly 5 percent of the time during summer months. Values near this limit should be treated with caution, as discussed in Section IV.A.

Table 9. DSS-34/35/36 expected array loss at 7.15 GHz, 20-deg elevation.

CD	Jan	Feb	Mar	Apr	May	Jun	Jul	Aug	Sep	Oct	Nov	Dec	Year Min	Year Avg	Year Max
0.00	0.001	0.001	0.001	0.001	0.000	0.000	0.000	0.002	0.000	0.000	0.000	0.001	0.000	0.001	0.002
0.10	0.011	0.010	0.008	0.005	0.003	0.004	0.004	0.004	0.006	0.004	0.009	0.010	0.003	0.006	0.011
0.20	0.019	0.016	0.015	0.009	0.006	0.007	0.007	0.009	0.012	0.009	0.015	0.016	0.006	0.011	0.019
0.25	0.025	0.019	0.020	0.011	0.007	0.008	0.008	0.012	0.015	0.011	0.019	0.020	0.007	0.014	0.025
0.30	0.030	0.023	0.025	0.014	0.009	0.010	0.011	0.016	0.019	0.014	0.023	0.024	0.009	0.017	0.030
0.40	0.043	0.031	0.036	0.021	0.013	0.015	0.016	0.026	0.028	0.023	0.035	0.034	0.013	0.026	0.043
0.50	0.062	0.043	0.053	0.031	0.020	0.021	0.025	0.041	0.040	0.034	0.051	0.049	0.020	0.038	0.062
0.60	0.091	0.061	0.076	0.047	0.029	0.032	0.039	0.061	0.057	0.051	0.073	0.073	0.029	0.056	0.091
0.70	0.137	0.089	0.116	0.073	0.044	0.044	0.064	0.088	0.083	0.080	0.108	0.113	0.044	0.085	0.137
0.80	0.218	0.142	0.183	0.119	0.076	0.079	0.109	0.137	0.126	0.131	0.181	0.207	0.076	0.139	0.218
0.85	0.291	0.190	0.241	0.156	0.105	0.103	0.145	0.178	0.166	0.177	0.247	0.287	0.103	0.186	0.291
0.90	0.410	0.271	0.348	0.226	0.148	0.139	0.204	0.237	0.228	0.246	0.367	0.442	0.139	0.265	0.442
0.91	0.445	0.295	0.378	0.248	0.159	0.149	0.220	0.254	0.245	0.267	0.400	0.499	0.149	0.288	0.499
0.92	0.485	0.326	0.412	0.266	0.171	0.164	0.239	0.275	0.262	0.288	0.446	0.543	0.164	0.314	0.543
0.93	0.532	0.358	0.454	0.295	0.190	0.179	0.260	0.298	0.291	0.314	0.495	0.605	0.179	0.346	0.605
0.94	0.588	0.395	0.508	0.320	0.207	0.198	0.282	0.327	0.316	0.347	0.567	0.677	0.198	0.382	0.677
0.95	0.649	0.450	0.567	0.362	0.233	0.222	0.315	0.364	0.354	0.389	0.658	0.748	0.222	0.430	0.748
0.96	0.752	0.516	0.649	0.414	0.269	0.259	0.349	0.410	0.394	0.437	0.751	0.865	0.259	0.490	0.865
0.97	0.867	0.608	0.758	0.484	0.312	0.304	0.402	0.472	0.444	0.509	0.906	1.021	0.304	0.573	1.021
0.98	1.095	0.785	0.944	0.595	0.400	0.383	0.468	0.571	0.527	0.657	1.093	1.281	0.383	0.713	1.281
0.99	1.501	1.124	1.152	0.780	0.602	0.586	0.629	0.703	0.735	0.873	1.446	1.682	0.586	0.964	1.682
0.995	1.936	1.369	1.525	1.092	0.797	0.741	0.777	0.872	0.979	1.123	1.884	2.179	0.741	1.254	2.179

Table 10. DSS-34/35 expected array loss at 7.15 GHz, 20-deg elevation.

CD	Jan	Feb	Mar	Apr	May	Jun	Jul	Aug	Sep	Oct	Nov	Dec	Year Min	Year Avg	Year Max
0.00	0.000	0.001	0.000	0.000	0.000	0.000	0.000	0.001	0.000	0.000	0.000	0.001	0.000	0.000	0.001
0.10	0.006	0.006	0.004	0.003	0.002	0.002	0.002	0.002	0.003	0.002	0.005	0.005	0.002	0.003	0.006
0.20	0.011	0.009	0.008	0.005	0.003	0.004	0.004	0.005	0.007	0.005	0.008	0.009	0.003	0.006	0.011
0.25	0.014	0.011	0.011	0.006	0.004	0.005	0.005	0.006	0.008	0.006	0.010	0.011	0.004	0.008	0.014
0.30	0.016	0.013	0.014	0.007	0.005	0.006	0.006	0.009	0.010	0.008	0.013	0.013	0.005	0.010	0.016
0.40	0.024	0.017	0.020	0.011	0.007	0.008	0.009	0.015	0.016	0.013	0.019	0.019	0.007	0.014	0.024
0.50	0.034	0.024	0.029	0.017	0.011	0.012	0.014	0.023	0.022	0.019	0.028	0.027	0.011	0.021	0.034
0.60	0.050	0.034	0.042	0.026	0.016	0.018	0.022	0.034	0.032	0.028	0.040	0.040	0.016	0.031	0.050
0.70	0.076	0.049	0.064	0.040	0.024	0.027	0.035	0.049	0.046	0.044	0.060	0.063	0.024	0.047	0.076
0.80	0.121	0.079	0.102	0.066	0.042	0.044	0.060	0.076	0.070	0.072	0.100	0.115	0.042	0.077	0.121
0.85	0.162	0.106	0.134	0.087	0.058	0.057	0.081	0.099	0.092	0.098	0.137	0.160	0.057	0.103	0.162
0.90	0.229	0.151	0.194	0.126	0.082	0.077	0.113	0.131	0.126	0.136	0.205	0.247	0.077	0.147	0.247
0.91	0.249	0.164	0.211	0.138	0.088	0.083	0.122	0.141	0.136	0.148	0.223	0.279	0.083	0.160	0.279
0.92	0.271	0.181	0.230	0.148	0.095	0.091	0.133	0.153	0.146	0.160	0.249	0.304	0.091	0.175	0.304
0.93	0.298	0.199	0.254	0.164	0.105	0.099	0.145	0.166	0.162	0.175	0.277	0.340	0.099	0.193	0.340
0.94	0.330	0.220	0.284	0.178	0.115	0.110	0.157	0.182	0.176	0.193	0.318	0.381	0.110	0.213	0.381
0.95	0.365	0.252	0.318	0.202	0.129	0.123	0.175	0.203	0.197	0.217	0.370	0.422	0.123	0.240	0.422
0.96	0.424	0.289	0.365	0.231	0.150	0.144	0.194	0.229	0.220	0.244	0.424	0.490	0.144	0.274	0.490
0.97	0.491	0.341	0.428	0.271	0.174	0.169	0.224	0.264	0.248	0.285	0.513	0.581	0.169	0.321	0.581
0.98	0.625	0.444	0.536	0.334	0.223	0.214	0.262	0.320	0.295	0.370	0.623	0.735	0.214	0.402	0.735
0.99	0.868	0.642	0.658	0.440	0.338	0.329	0.353	0.396	0.415	0.494	0.835	0.979	0.329	0.548	0.979
0.995	1.137	0.788	0.883	0.623	0.450	0.418	0.439	0.494	0.556	0.642	1.104	1.291	0.418	0.719	1.291

Table 11. DSS-34/36 expected array loss at 7.15 GHz, 20-deg elevation.

CD	Jan	Feb	Mar	Apr	May	Jun	Jul	Aug	Sep	Oct	Nov	Dec	Year Min	Year Avg	Year Max
0.00	0.001	0.002	0.001	0.001	0.000	0.000	0.000	0.003	0.000	0.000	0.000	0.001	0.000	0.001	0.003
0.10	0.013	0.012	0.010	0.006	0.004	0.004	0.004	0.005	0.007	0.005	0.010	0.012	0.004	0.007	0.013
0.20	0.024	0.020	0.019	0.010	0.007	0.008	0.008	0.010	0.014	0.010	0.018	0.020	0.007	0.014	0.024
0.25	0.030	0.024	0.024	0.013	0.009	0.010	0.010	0.014	0.018	0.014	0.023	0.024	0.009	0.017	0.030
0.30	0.037	0.028	0.030	0.017	0.011	0.012	0.013	0.019	0.023	0.017	0.028	0.029	0.011	0.021	0.037
0.40	0.053	0.038	0.044	0.025	0.016	0.018	0.020	0.032	0.035	0.028	0.043	0.042	0.016	0.032	0.053
0.50	0.076	0.052	0.064	0.037	0.024	0.026	0.031	0.050	0.049	0.041	0.062	0.060	0.024	0.046	0.076
0.60	0.111	0.074	0.093	0.057	0.036	0.039	0.048	0.075	0.070	0.063	0.089	0.089	0.036	0.069	0.111
0.70	0.167	0.108	0.142	0.089	0.054	0.060	0.078	0.107	0.101	0.098	0.132	0.138	0.054	0.104	0.167
0.80	0.264	0.173	0.223	0.145	0.093	0.096	0.133	0.166	0.154	0.159	0.220	0.251	0.093	0.169	0.264
0.85	0.351	0.231	0.292	0.190	0.128	0.125	0.177	0.216	0.202	0.215	0.299	0.347	0.125	0.226	0.351
0.90	0.491	0.327	0.419	0.274	0.179	0.170	0.248	0.287	0.276	0.297	0.442	0.529	0.170	0.320	0.529
0.91	0.532	0.356	0.454	0.300	0.194	0.181	0.266	0.307	0.296	0.322	0.480	0.595	0.181	0.348	0.595
0.92	0.579	0.392	0.494	0.322	0.208	0.199	0.289	0.332	0.317	0.348	0.533	0.645	0.199	0.378	0.645
0.93	0.633	0.430	0.542	0.356	0.231	0.217	0.314	0.359	0.351	0.379	0.591	0.716	0.217	0.416	0.716
0.94	0.697	0.473	0.605	0.386	0.252	0.240	0.341	0.394	0.380	0.417	0.673	0.798	0.240	0.459	0.798
0.95	0.766	0.538	0.673	0.435	0.282	0.269	0.380	0.438	0.426	0.466	0.777	0.877	0.269	0.514	0.877
0.96	0.881	0.614	0.766	0.496	0.325	0.314	0.420	0.491	0.472	0.523	0.880	1.006	0.314	0.585	1.006
0.97	1.008	0.720	0.888	0.578	0.377	0.366	0.482	0.564	0.531	0.606	1.049	1.173	0.366	0.680	1.173
0.98	1.250	0.918	1.090	0.705	0.480	0.460	0.559	0.678	0.627	0.776	1.247	1.438	0.460	0.838	1.438
0.99	1.650	1.280	1.308	0.912	0.713	0.695	0.743	0.826	0.863	1.014	1.598	1.814	0.695	1.112	1.814
0.995	2.029	1.524	1.673	1.247	0.931	0.869	0.909	1.013	1.128	1.279	1.987	2.216	0.869	1.411	2.216

Table 12. DSS-35/36 expected array loss at 7.15 GHz, 20-deg elevation.

CD	Jan	Feb	Mar	Apr	May	Jun	Jul	Aug	Sep	Oct	Nov	Dec	Year Min	Year Avg	Year Max
0.00	0.000	0.001	0.000	0.000	0.000	0.000	0.000	0.001	0.000	0.000	0.000	0.000	0.000	0.000	0.001
0.10	0.005	0.005	0.004	0.002	0.001	0.002	0.002	0.002	0.003	0.002	0.004	0.005	0.001	0.003	0.005
0.20	0.009	0.008	0.007	0.004	0.003	0.003	0.003	0.004	0.006	0.004	0.007	0.008	0.003	0.005	0.009
0.25	0.012	0.009	0.009	0.005	0.003	0.004	0.004	0.006	0.007	0.005	0.009	0.009	0.003	0.007	0.012
0.30	0.014	0.011	0.012	0.006	0.004	0.005	0.005	0.007	0.009	0.007	0.011	0.011	0.004	0.008	0.014
0.40	0.020	0.015	0.017	0.010	0.006	0.007	0.008	0.012	0.013	0.011	0.017	0.016	0.006	0.012	0.020
0.50	0.029	0.020	0.025	0.014	0.009	0.010	0.012	0.020	0.019	0.016	0.024	0.023	0.009	0.018	0.029
0.60	0.043	0.029	0.036	0.022	0.014	0.015	0.019	0.029	0.027	0.024	0.035	0.035	0.014	0.027	0.043
0.70	0.065	0.042	0.055	0.035	0.021	0.023	0.030	0.042	0.039	0.038	0.051	0.054	0.021	0.040	0.065
0.80	0.104	0.068	0.087	0.056	0.036	0.038	0.052	0.065	0.060	0.062	0.086	0.099	0.036	0.066	0.104
0.85	0.139	0.091	0.115	0.074	0.050	0.049	0.069	0.085	0.079	0.084	0.118	0.137	0.049	0.089	0.139
0.90	0.197	0.130	0.167	0.108	0.070	0.066	0.097	0.113	0.109	0.117	0.176	0.213	0.066	0.127	0.213
0.91	0.214	0.141	0.181	0.118	0.076	0.071	0.105	0.121	0.117	0.127	0.192	0.241	0.071	0.138	0.241
0.92	0.234	0.156	0.198	0.127	0.082	0.078	0.114	0.131	0.125	0.138	0.215	0.263	0.078	0.150	0.263
0.93	0.257	0.172	0.219	0.141	0.091	0.085	0.124	0.143	0.139	0.151	0.239	0.293	0.085	0.166	0.293
0.94	0.285	0.190	0.245	0.154	0.099	0.094	0.135	0.157	0.151	0.166	0.274	0.329	0.094	0.184	0.329
0.95	0.315	0.217	0.275	0.174	0.111	0.106	0.151	0.175	0.170	0.187	0.320	0.365	0.106	0.207	0.365
0.96	0.367	0.249	0.315	0.199	0.129	0.124	0.167	0.197	0.189	0.210	0.367	0.424	0.124	0.237	0.424
0.97	0.425	0.295	0.370	0.234	0.150	0.145	0.193	0.228	0.214	0.246	0.445	0.504	0.145	0.277	0.504
0.98	0.543	0.384	0.464	0.288	0.192	0.184	0.226	0.277	0.255	0.319	0.541	0.640	0.184	0.347	0.640
0.99	0.758	0.558	0.572	0.381	0.292	0.284	0.305	0.342	0.358	0.428	0.728	0.857	0.284	0.475	0.857
0.995	1.000	0.687	0.771	0.541	0.390	0.361	0.379	0.428	0.482	0.557	0.970	1.141	0.361	0.626	1.141

Table 13. DSS-34/35 expected array loss at 34/5 GHz, 20-deg elevation.

CD	Jan	Feb	Mar	Apr	May	Jun	Jul	Aug	Sep	Oct	Nov	Dec	Year Min	Year Avg	Year Max
0.00	0.006	0.016	0.010	0.006	0.003	0.002	0.003	0.029	0.005	0.004	0.005	0.013	0.002	0.007	0.029
0.10	0.138	0.127	0.102	0.061	0.040	0.046	0.045	0.050	0.075	0.056	0.108	0.124	0.040	0.077	0.138
0.20	0.242	0.200	0.190	0.108	0.073	0.083	0.083	0.108	0.149	0.109	0.185	0.205	0.073	0.140	0.242
0.25	0.306	0.243	0.245	0.139	0.091	0.105	0.107	0.149	0.189	0.141	0.233	0.248	0.091	0.177	0.306
0.30	0.368	0.283	0.304	0.171	0.111	0.128	0.134	0.198	0.233	0.179	0.289	0.295	0.111	0.218	0.368
0.40	0.521	0.386	0.442	0.256	0.164	0.182	0.205	0.326	0.348	0.286	0.426	0.417	0.164	0.322	0.521
0.50	0.727	0.517	0.626	0.376	0.245	0.261	0.314	0.499	0.487	0.411	0.606	0.590	0.245	0.462	0.727
0.60	1.019	0.716	0.876	0.563	0.359	0.393	0.476	0.721	0.675	0.612	0.844	0.844	0.359	0.665	1.019
0.70	1.425	0.997	1.253	0.844	0.530	0.587	0.743	0.989	0.938	0.916	1.180	1.224	0.530	0.961	1.425
0.80	1.976	1.468	1.766	1.272	0.872	0.903	1.191	1.423	1.339	1.375	1.750	1.916	0.872	1.442	1.976
0.85	2.327	1.812	2.102	1.576	1.150	1.128	1.493	1.729	1.649	1.723	2.131	2.311	1.128	1.783	2.327
0.90	2.674	2.243	2.522	2.025	1.509	1.445	1.897	2.079	2.032	2.125	2.575	2.736	1.445	2.215	2.736
0.91	2.740	2.341	2.602	2.135	1.597	1.522	1.988	2.164	2.119	2.224	2.654	2.818	1.522	2.314	2.818
0.92	2.801	2.452	2.680	2.222	1.682	1.629	2.091	2.259	2.203	2.314	2.741	2.866	1.629	2.411	2.866
0.93	2.855	2.550	2.755	2.341	1.810	1.737	2.194	2.353	2.327	2.414	2.814	2.914	1.737	2.514	2.914
0.94	2.903	2.641	2.829	2.434	1.917	1.859	2.292	2.457	2.418	2.517	2.886	2.951	1.859	2.613	2.951
0.95	2.938	2.749	2.887	2.561	2.060	2.001	2.416	2.567	2.539	2.628	2.943	2.973	2.001	2.713	2.973
0.96	2.974	2.838	2.938	2.684	2.235	2.191	2.524	2.674	2.639	2.727	2.974	2.994	2.191	2.808	2.994
0.97	2.994	2.916	2.976	2.799	2.406	2.374	2.658	2.783	2.738	2.830	2.998	3.005	2.374	2.891	3.005
0.98	3.007	2.982	3.001	2.907	2.654	2.616	2.777	2.890	2.850	2.942	3.007	3.010	2.616	2.964	3.010
0.99	3.010	3.008	3.008	2.981	2.912	2.901	2.928	2.960	2.970	2.995	3.010	3.010	2.901	3.002	3.010
0.995	3.010	3.010	3.010	3.007	2.984	2.972	2.980	2.995	3.003	3.008	3.010	3.010	2.972	3.009	3.010

V. Conclusion

This article provides sufficient information about atmospheric decorrelation to enable a flight project to statistically account for this effect in the design of a telecommunications link involving two or more arrayed antennas in the DSN at the X-band and Ka-band frequencies. Predictions in the form of monthly and annual cumulative distributions of the phasing loss have been derived from the data acquired by the site test interferometers. These phasing loss statistics are given for selected two-element and three-element array configurations at the DSN uplink frequencies of 7.15 GHz and 34.5 GHz and at an elevation angle of 20 deg for both Goldstone and Canberra DSN sites. We have also discussed validation tests that ensure the integrity of the STI data.

Acknowledgments

References

[1] D. D. Morabito, L. R. D'Addario, R. Acosta, and J. Nessel, "An Inter-Comparison of Two Independent Site Test Interferometers Located in Goldstone, California: Initial Study Results," *Proceedings of the Ka and Broadband Communications, Navigation and Earth Observation Conference*, Ottawa, Canada, September 2012.

[2] D. D. Morabito, L. R. D'Addario, R. J. Acosta, and J. A. Nessel, "Tropospheric Delay Statistics Measured by Two Site Test Interferometers at Goldstone, California," *Radio Science*, vol. 48, no. 6, pp. 729–738, November/December 2013.
http://onlinelibrary.wiley.com/doi/10.1002/2013RS005268/abstract

[3] S. D. Slobin, "Atmospheric and Environmental Effects," *DSN Telecommunications Link Design Handbook*, DSN No. 810-005, Space Link Interfaces, Module 105, Rev. D, Jet Propulsion Laboratory, Pasadena, California, September 15, 2009.
http://deepspace.jpl.nasa.gov/dsndocs/810-005/105/105D.pdf

[4] D. D. Morabito and L. D'Addario, "Two-Element Uplink Array Loss Statistics Derived from Site Test Interferometer Phase Data for the Goldstone Climate: Initial Study Results," *The Interplanetary Network Progress Report*, vol. 42-186, Jet Propulsion Laboratory, Pasadena, California, pp. 1–20, August 15, 2011.
http://ipnpr.jpl.nasa.gov/progress_report/42-186/186B.pdf

[5] S. D. Slobin, "70-m Subnet Telecommunications Interfaces," *DSN Communications Link Design Handbook*, DSN No. 810-005, Space Link Interfaces, Module 101, Rev. D, Jet Propulsion Laboratory, Pasadena, California, April 21, 2011.
http://deepspace.jpl.nasa.gov/dsndocs/810-005/101/101D.pdf

[6] S. D. Slobin, "34-m HEF Subnet Telecommunications Interfaces," *DSN Telecommunications Link Design Handbook*, DSN No. 810-005, Space Link Interfaces, Module 103, Rev. B, Jet Propulsion Laboratory, Pasadena, California, September 19, 2008.
http://deepspace.jpl.nasa.gov/dsndocs/810-005/103/103B.pdf

[7] S. D. Slobin, "34-m BWG Stations Telecommunications Interfaces," *DSN Telecommunications Link Design Handbook*, DSN No. 810-005, Space Link Interfaces, Module 104, Rev. G, Jet Propulsion Laboratory, Pasadena, California, March 5, 2013.
http://deepspace.jpl.nasa.gov/dsndocs/810-005/104/104G.pdf

[8] R. S. Kimberk, T. R. Hunter, P. S. Leiker, R. Blundell, G. U. Nystrom, G. R. Petitpas, J. Test, R. W. Wilson, P. Yamaguchi, and K. H. Young, "A Multi-Baseline 12 GHz Atmospheric Phase Interferometer with One Micron Path Length Sensitivity," *Journal of Astronomical Instrumentation*, vol. 1, no. 1, July 31, 2012.
http://www.worldscientific.com/doi/pdf/10.1142/S225117171250002X

[9] L. R. D'Addario, "Combining Loss of a Transmitting Array due to Phase Errors," *The Interplanetary Network Progress Report*, vol. 42-175, Jet Propulsion Laboratory, Pasadena, California, pp. 1–7, November 15, 2008.
http://ipnpr.jpl.nasa.gov/progress_report/42-175/175G.pdf

[10] R. N. Treuhaft and G. E. Lanyi, "The Effect of the Dynamic Wet Troposphere on Radio Interferometric Measurements," *Radio Science*, vol. 22, no. 2, pp. 251–265, March–April 1987.
http://www.agu.org/pubs/crossref/1987/RS022i002p00251.shtml

[11] R. W. Sniffen, "Coverage and Geometry," *DSN Communications Link Design Handbook*, DSN No. 810-005, Ground Station Properties, Module 301, Rev. H, Jet Propulsion Laboratory, Pasadena, California, October 17, 2012.
http://deepspace.jpl.nasa.gov/dsndocs/810-005/301/301H.pdf

[12] D. D. Morabito, L. D'Addario, S. Shambayati, R. J. Acosta, and J. A. Nessel, J. A., "Goldstone Site Test Interferometer Atmospheric Decorrelation Statistics Use in Spacecraft Link Budgets: First Year of STI Data," *Proceedings of the 14th Ka and Broadband Communications Conference*, Matera, Italy, September 24-26, 2008.

[13] D. D. Morabito, L. R. D'Addario, S. Keihm, and S. Shambayati, "Comparison of Dual Water Vapor Radiometer Differenced Path Delay Fluctuations and Site Test Interferometer Phase Delay Fluctuations Over a Shared 250-Meter Baseline," *The Interplanetary Network Progress Report*, vol. 42-188, Jet Propulsion Laboratory, Pasadena, California, pp. 1–21, February 15, 2012.
http://ipnpr.jpl.nasa.gov/progress_report/42-188/188A.pdf

[14] V. Vilnrotter, D. Lee, T. Cornish, R. Mukai, and L. Paal, "Uplink Arraying Experiment with the Mars Global Surveyor Spacecraft," *The Interplanetary Network Progress Report*, vol. 42-166, Jet Propulsion Laboratory, Pasadena, California, pp. 1–21, August 15, 2006.
http://ipnpr.jpl.nasa.gov/progress_report/42-166/166F.pdf

[15] V. A. Vilnrotter, P. C. Tsao, D. K. Lee, T. P. Cornish, L. Paal, and V. Jamnejad, "EPOXI Uplink Array Experiment of June 27, 2008, *The Interplanetary Network Progress Report*, vol. 42-174, Jet Propulsion Laboratory, Pasadena, California, pp. 1–25, August 15, 2008.
http://ipnpr.jpl.nasa.gov/progress_report/42-174/174E.pdf

[16] V. Vilnrotter, D. Lee, T. Cornish, P. Tsao, L. Paal, and V. Jamnejad, "Uplink Array Concept Demonstration with the EPOXI Spacecraft, *Proceedings of the 2009 IEEE Aerospace Conference*, paper 4.0101, Big Sky, Montana, March 7–14, 2009.

[17] R. J. Acosta, J. A. Nessel, I. K. Bibyk, B. Frantz, and D. D. Morabito, "Measurements of K-Band Carrier Amplitude and Phase Fluctuations Due to Atmospheric Effects Via Interferometry," *Proceedings of the 12th Ka and Broadband Communications Conference*, Naples, Italy, September 27–29, 2006.

[18] R. J. Acosta, B. Frantz, J. A. Nessel, and D. D. Morabito, "Goldstone Site Test Interferometer," *Proceedings of the 13th Ka and Broadband Communications Conference*, Turin, Italy, September 24–26, 2007.

[19] R. J. Acosta, J. A. Nessel, and D. D. Morabito, "Data Processing for Atmospheric Phase Interferometers," *Proceedings of the 14th Ka and Broadband Communications Conference*, Matera, Italy, September 24–26, 2008.

[20] J. A. Nessel, R. J. Acosta, and D. D. Morabito, "Goldstone Site Test Interferometer Phase Stability Analysis," *Proceedings of the 13th Ka and Broadband Communications Conference*, Turin, Italy, September 24–26, 2007.

[21] J. A. Nessel, R. J. Acosta, and D. D. Morabito, "Phase Fluctuations at Goldstone Derived From One-Year Site Testing Interferometer Data," *Proceedings of the 14th Ka and Broadband Communications Conference*, Matera, Italy, September 24–26, 2008.